Thermoacoustic amplification of photoacoustic signal

F. G. C. Bijnen, J. v. Dongen, J. Reuss, and F. J. M. Harren
Department of Molecular and Laser Physics, University of Nijmegen, Toernooiveld, 6525 ED Nijmegen, the Netherlands

(Received 28 December 1995; accepted for publication 26 February 1996)

The thermoacoustic effect is used to amplify the photoacoustic signal induced by trace gas absorption of CO_2 laser radiation. The acoustic wave pattern in a thermoacoustic amplifier coupled to a photoacoustic cell is represented in terms of electric transmission lines. Predictions of this model have resulted in a prototype thermoacoustic–photoacoustic (TAPA) detector to get a better understanding of this combination. The photoacoustic signal strength of the TAPA cell was linear with the trace gas density in the cell. Within this study we observed for the TAPA cell a higher PA signal than generated by a normal PA cell. Design criteria for better thermoacoustic amplification of photoacoustic signal are discussed. © *1996 American Institute of Physics.* [S0034-6748(96)00906-9]

I. INTRODUCTION

Photoacoustics (PA) has gained momentum by the invention of lasers and is used among others as a way to monitor on-line trace gas amounts of specific gases or volatiles[1–5] at part per billion and part per trillion level (1 ppb$=1\times10^{9}$ and 1 ppt$=1\times10^{12}$, respectively) with a time response of only a few seconds.[6,7] Detection limits are currently determined by electronic noise from the microphone, acoustic noise, or photoacoustic signals from other sources, e.g., cell windows or walls or other (unknown) gases; the latter are generally called background signals. Ultimately the detection limit is determined by noise due to Brownian motion of molecules near the membrane of the microphone.[8] By choosing an optimal, resonant cell design the PA signal can be amplified.[2–5,7,9–11] This type of passive resonant amplification is limited mainly by thermal and viscous losses near the resonator wall. Active thermoacoustic (TA) amplification of the PA signal can overcome these losses and improves the quality factor of the resonator, and consequently it enhances the PA signal.

Both TA and PA represent areas in physics which are described already more than 100 years ago by Lord Rayleigh[12] and Bell,[13] respectively. Recently, a first example of the combined effect has been described to monitor small absorptions.[14] For trace gas analysis the advantage of TAPA cell design becomes manifest when the noise of the microphone (electrical, phonon noise in the membrane) is limiting.

Thermoacoustics is well known to glass blowers; if the closed end of a quartz tube is heated in a flame and the open side is kept at ambient temperature a sound can be heard corresponding to the resonance frequency of the tube. Also physicists working with liquid helium can observe this effect; there it is known as ''Taconis oscillations.''[15] TA has recently found an application as the cooling mechanism in a refrigerator working on sound. Since no chemicals are needed such a device has been sent into space by NASA.[16] In our application we use the reverse process; the conversion of heat onto sound (prime mover).

The operating principle of the TA amplifier connected to a PA resonator can be explained as follows. The gas inside the acoustical resonator is irradiated by an amplitude modulated laser beam, the modulation frequency of which should coincide with the overall resonance frequency of combined resonator and amplifier (Fig. 1): Trace gas absorption inside the resonator tube will produce a standing acoustical wave; this is the acoustic effect. By adjusting the TA amplifier just below the onset of self-oscillation, the acoustical wave in the resonator will put the amplifier in sustained oscillation, leading to a considerable enhancement of the PA signal strength.

The PA signal generated in a longitudinal resonant cell will be treated in terms of a transmission line model.[7,17,18] The recently developed description of the TA effect below the onset of self-oscillation,[16,19] is implemented in the transmission line model. Calculated values are compared with the performance of the prototype TAPA cell. Some design criteria for optimal TA amplification of PA signal are discussed.

II. THEORY

An acoustic wave transmitted through a tube can be described analytically in the one-dimensional electric transmission line analog.[17] In the field of PA spectroscopy this model has been described earlier and was extended with a matrix formalism to permit a quantitative description of the PA signal as function of position in the PA cell and frequency of the resonator.[7,18] We will shortly summarize this model, and then express thermoacoustics in terms of the same transmission line model. A brief explanation of thermoacoustics will be given, explaining how temperature gradients can induce amplification of acoustic waves.

A. Photoacoustic transmission line model

Within the transmission line description of acoustic waves the properties of ducts forming a PA cell can be expressed as discrete circuit immittances per unit length, such as susceptance, conductance, resistance, and reactance (see Table I).[7,17,18] These immittances assume piecewise constant values. Introducing a source of sound due to trace gas absorption of modulated laser energy yields periodical and spatially varying changes of pressure $p(x)$. The electric analog of the sound pressure $p(x)$ is the voltage $V(x)$; the analog of the total gas flux $Su(x)$ [cross section $S\times$ velocity $u(x)$] is the electric current $I(x)$. The immittances reflect the energy

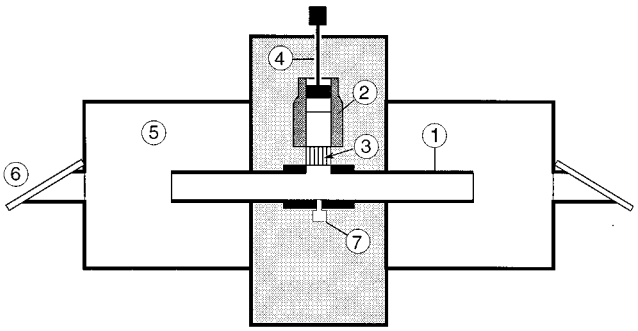

FIG. 1. Photoacoustic cell with thermoacoustic amplifier positioned onto the acoustic resonator. 1: Acoustic resonator at ambient temperature; 2: high temperature column (300–475 K); 3: combined stainless steel and copper stacks with temperature gradient ΔT; 4: tunable piston to change high temperature column L_{T_h}; 5: buffer volume; 6: Brewster window; 7: microphone.

contents of the acoustic wave (due to movement and compression) and the losses (viscous and thermal).

Surface losses can be calculated from the thermal and viscous boundary layers of the gas near the duct wall (volume losses are neglected). The thicknesses of these boundary layers are given by[17]

$$\delta_\kappa = \sqrt{\frac{2\kappa}{\rho_m \omega c_p}} \quad \text{and} \quad \delta_\nu = \sqrt{\frac{2\nu}{\rho_m \omega}} \tag{1}$$

with κ the coefficient of heat conduction, ρ_m the mean gas mass density, ω the angular oscillation frequency, c_p the heat capacity per unit mass, and ν the dynamic viscosity of the gas.

The differential equations for the waves in a duct in the formalism of the electrical transmission line are given by[7,18]

$$\frac{dV(x)}{dx} = ZI(x) \quad \text{and} \quad \frac{dI(x)}{dx} = -V(x)Y + V_0 Y. \tag{2}$$

Expressions for the impedance Z, the admittance Y, and the source term (absorption strength) V_0 are given in Table I; x is the propagation direction of the waves. The solutions of the differential equations are

$$V(x) = V_0 - Z_c(A\ e^{\beta x} - B\ e^{-\beta x}) \text{ and } I(x) = A\ e^{\beta x} + B\ e^{-\beta x} \tag{3}$$

with $\beta = \sqrt{ZY}$ the propagation constant and $Z_c = \sqrt{Z/Y}$ the characteristic impedance of the transmission line. The amplitudes A and B are determined by the requirement of the continuity of gas flux $I(x)$ and the pressure $V(x)$ at the boundaries between two connected ducts.

TABLE I. Transmission line parameters: D is the perimeter and S the cross sectional area of the duct, Pa_g is the partial pressure of the gas, P_L is the unmodulated power of the incident laser beam, and c the velocity of sound. The other parameters are explained in the text.

Resistance (viscous losses)	$R = \rho_m \omega \delta_\nu D/2S^2$
Inductance (kinetic energy)	$\omega L = \omega \rho_m / S$
Conductance (heat conduction losses)	$G = (\gamma - 1)\omega \delta_\kappa D/2\rho_m c^2$
Susceptance (potential energy)	$\omega C = \omega S/\rho_m c^2$
Impedance	$Z = R + i\omega L$
Admittance	$Y = G + i\omega C$
Source term (absorbed laser power converted to sound)	$V_0 = (\gamma - 1) P a_g P_L \alpha / i\omega S$

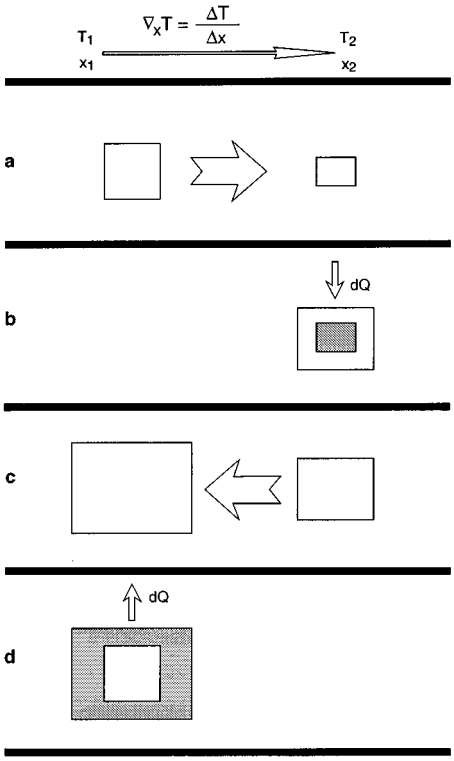

FIG. 2. Schematical view of the thermodynamic cycle of an air parcel traveling along a plate with temperature gradient ΔT. During each cycle of (externally induced) acoustic oscillations, the parcel is compressed (step a) as it is pushed from x_1 toward x_2. At x_2 an amount of heat (dQ) is absorbed (step b). During expansion (step c) the parcel returns to its initial position x_1. Here, finally it releases the excess heat (dQ).

B. General description of the thermoacoustic effect

A review on TA engines is given by Swift.[16] In Fig. 2 the periodical motion of a gas parcel in a longitudinal sound wave is depicted schematically as a cycle with four discrete steps; in reality the changes occur more gradually. In Fig. 3(a) the same discrete process is depicted in a thermodynamic cycle. The parcel is close to a wall along which a external temperature gradient ΔT maintains. If the parcel is within the thermal boundary layer δ_κ, a good thermal heat exchange with the wall takes place. Consider the parcel at position x_1 at T_1 (see Fig. 2). Due to the standing acoustical wave maintained in the system the parcel is compressed adiabatically in moving from x_1 to x_2 [step a in Figs. 2 and 3(a)]. During step b the parcel accommodates to the increased temperature T_2 by isobaric expansion; an amount of energy dQ is transported from the plate toward the parcel. During the second half of the period (step c) the parcel moves back to x_1, during which it expands adiabatically to its initial pressure. However, its volume and temperature are still larger than at to the starting position of step a. In step d the parcel resumes isobarically the temperature of the plate T_1; its volume decreases to its starting value with the excess of energy dQ flowing back to the plate.

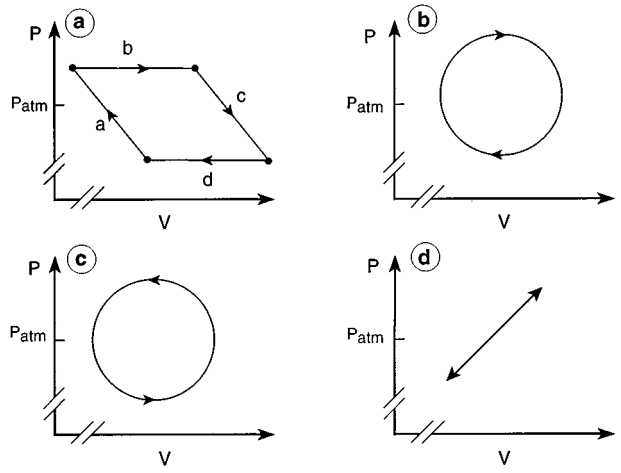

FIG. 3. Carnot cycles in various circumstances. (a) Thermodynamic process as presented in Fig. 2 in four discrete steps: (a) and (c) adiabatic compression and expansion, (b) and (d) isobaric expansion and compression, respectively. (b) Continuous changing representation of the thermodynamic behavior of the gas parcel (a) within the thermal boundary layer δ_κ and ΔT large. The gas does network (''prime mover''). (c) If ΔT is small at a distance δ_κ from the plate and the gas parcel absorbs work and transfers this into heat (heat pump). (d) Far from the plate or very close to the plate no network is done or absorbed (neglecting volume losses).

Thus, during this thermodynamic cycle work is done by the parcel [$\oint P\,dV \geqslant 0$, Fig. 3(a)]. Heat is transported from the high temperature side (x_2) to the cold side (x_1) of the plate. The equivalent continuous process is depicted in Fig. 3(b). If no (or only a small) temperature gradient is present acoustic energy is lost and converted into viscous and thermal losses at the plate [$\oint P\,dV \leqslant 0$, Fig. 3(c)]. At a distance from the plate much larger than the boundary layer thickness no energy is dissipated to the wall and the wave expands and compresses adiabatically [$\oint P\,dV = 0$, Fig. 3(d); neglecting volume losses].

C. Representation of the thermoacoustic effect in the transmission line model

The formulas expressing the relationship between the pressure $p(x)$ and velocity $u(x)$ for the standing acoustic wave in a TA stack have been derived and reviewed for the general case.[16] More recently, a description has been given for a stack operated below the self-oscillation threshold.[19] Here we take up the resulting differential equations of that analysis and present an analytical solution which is implemented in the transmission line model for acoustic waves.

The TA stack consists of metal plates at a distance of approximately two times the thermal boundary layer. The relations for the pressure and velocity of air parcels along such a stack with temperature gradient $\nabla_x T$ are given by[19]

$$\frac{dp(x)}{dx} = \frac{-i\omega\rho_m}{(1-f_\nu)}\,u(x)$$

and

$$\frac{du(x)}{dx} = \frac{i}{\omega\rho_m}\,\frac{(f_\kappa - f_\nu)}{(1-\sigma)(1+\epsilon_s)}\,\frac{\nabla_x T}{T_m}\,\frac{dp(x)}{dx} - \frac{i}{\omega\rho_m}\,\frac{\omega^2}{c^2}\left[1+\frac{(\gamma-1)}{(1+\epsilon_s)}\,f_\kappa\right]p(x) \tag{4}$$

with $\sigma = c_p\nu/\kappa$ the Prandtl number and T_m the average temperature of the gas. f_κ, f_ν, and ϵ_s are given by

$$f_\kappa = \frac{\tanh\{(1+i)y_0/\delta_\kappa\}}{(1+i)y_0/\delta_\kappa},$$

$$f_\nu = \frac{\tanh\{(1+i)y_0/\delta_\nu\}}{(1+i)y_0/\delta_\nu}, \tag{5}$$

$$\epsilon_s = \frac{\rho_m c_p \delta_\kappa \tanh\{(1+i)y_0/\delta_\kappa\}}{\rho_s c_s \delta_s \tanh\{(1+i)l_s/\delta_s\}}$$

with $2y_0$ the stack plate spacing, $2l_s$ the thickness of the stack plates, c_s the heat capacity per unity mass for the plate material, and ρ_s the density of the plates. The thickness of the thermal boundary layer within the plates (δ_s) is given by $\delta_s = \sqrt{2\kappa_s/\rho_s c_s \omega}$ with κ_s the heat conductivity of the solid.

The solution for the differential equations [Eqs. (4)] in the transmission line representation of acoustic waves is given by

$$V(x) = -Z_{c^+} A\,e^{\beta_+ x} + Z_{c^-} B\,e^{-\beta_- x} \tag{6}$$

and

$$I(x) = A\,e^{\beta_+ x} + B\,e^{-\beta_- x} \tag{7}$$

with $\beta_\pm$ the propagation constants in both directions and $Z_{c^\pm}$ the characteristic impedances given by

$$\beta_\pm = i\sqrt{\frac{\omega^2}{c^2}\,\frac{[1+\epsilon_s+(\gamma-1)f_\kappa]}{(1-f_\nu)(1+\epsilon_s)} - \left[\frac{f_\kappa - f_\nu}{2(1-f_\nu)(1-\sigma)(1+\epsilon_s)}\,\frac{\nabla_x T}{T_m}\right]^2} \pm \frac{f_\kappa - f_\nu}{2(1-f_\nu)(1-\sigma)(1+\epsilon_s)}\,\frac{\nabla_x T}{T_m},$$

and

$$Z_{c^\pm} = \frac{i\omega\rho_m}{(1-f_\nu)S\beta_\pm}. \tag{8}$$

As before the values for A and B are determined by the continuity conditions at the interfaces between differently shaped ducts.

The combined TAPA cell is shown schematically in Figs. 1 and 4. Starting from the center of the longitudinal resonator the TA amplifier consists of a part at ambient tem-

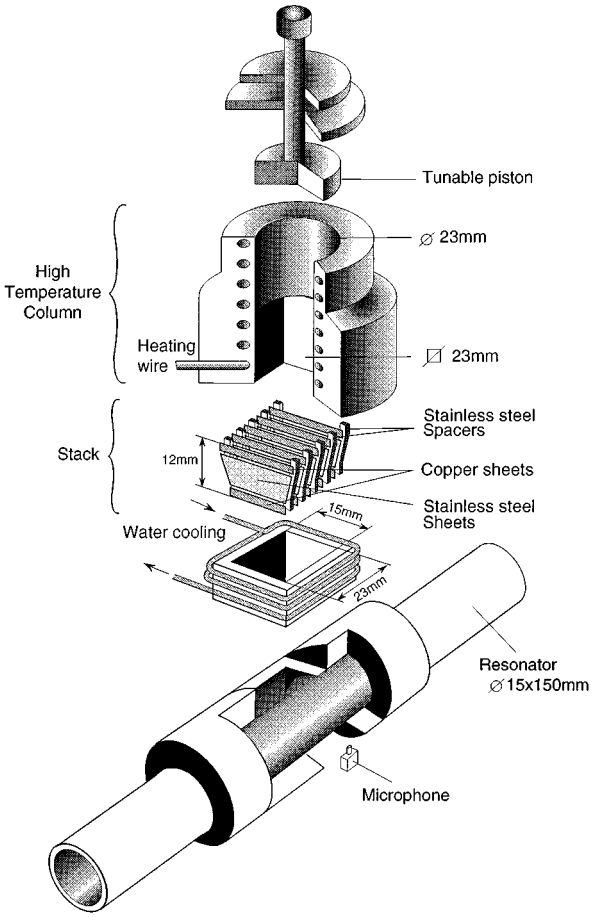

FIG. 4. Expanded view of the thermoacoustic stack, dimensions are in mm. The tunable piston can slide in the upper part of the column which is cylindrically shaped (diameter 23 mm). The lower part (length 20 mm, square cross section 23×23 mm) forms the connection to the stack. This part is heated by ''Inconel'' wire. The exploded view of the stack show the stainless steel plates with the temperature gradient and copper plates to maintain the gradient; stainless steel spacers separate the plates. At the connection between thermoacoustic stack and the photoacoustic resonator water cooling removes the excess in heat and keeps the lower end of the stack at constant temperature.

perature, T_a, a composite stack and a part at high temperature, T_h, which can be varied in length; this length adjustment was added to the amplifier to confirm experimentally the result from the model. The composite stack consists of three parts; a stack of copper (high κ) plates at the lower and upper sides to achieve uniform temperature distributions over the cross section of the tube. The central stack contains stainless steel (low κ) plates of height h_{ss} over which the temperature gradient, $\nabla_x T=(T_h-T_a)/h_{ss}$.

Within the transmission line model the TA amplifier will be represented as a single input impedance connected to the central transmission line formed by resonator and buffers. To quantify this impedance each part of the amplifier has to be described separately.

The amplifier, without the composite stack, is represented by the ordinary solutions of the differential equations [Eq. (3)]. The solution and differential equations for an acoustic wave along the temperature gradient over the central stainless steel stack are given by Eq. (8). Since no temperature gradient is assumed along the copper plates (high thermal conductivity) Eq. (8) can also for these with the restriction that $\nabla_x T=0$.

Coupling of the five different parts of the amplifier is achieved most conveniently in the matrix formalism.[7,18] Multiplication of the matrices and fulfilling the boundary conditions (closed end at the high temperature part) result in an expression for the input impedance of the amplifier (Z_{TA}) which is inserted in the central transmission line at the middle of the resonator.

III. EXPERIMENT

Experiments have been performed with the TAPA cell by varying the temperature and the length of the high temperature column (L_{T_h}). One set of experiments was obtained by employing a small external loudspeaker mounted at the position of one Brewster window.

The PA signal was generated through excitation of trace amounts of ethylene with a CO_2 laser operating at the 10P14 (949.48 cm^{-1}) or 10P16 (947.74 cm^{-1}) laser line; absorption coefficients for ethylene on these laser lines are 30.4 and 5.07 $atm^{-1}\,cm^{-1}$, respectively.[20] Amplitude modulation of the laser beam at the resonance frequency of the TAPA cell (≈600 Hz) was achieved by a stabilized chopper with a long term stability of 0.1 Hz. A 5 L/h flow of N_2 containing trace amounts of ethylene passed through the resonator kept at ambient pressure. The generated acoustical signals were detected by a small microphone (Knowless EK 3024) and processed by a lock-in amplifier.

The longitudinal acoustic resonator, a gold coated brass tube (diameter 15 mm, length 150 mm), was separated from the Brewster windows by buffer volumes (diameter 100 mm, length 100 mm, Fig. 4). At the central part of the resonator two holes were drilled (diameter 0.8 mm) opposite each other to allow connection of the microphone and the gas inlet. A large hole (15×23 mm) perpendicular to these forms the connection to the TA amplifier. The total height of the combined stack of copper and stainless steel plates was 12 mm; the thickness of the plates was 50 μm and they were separated by a distance of 300 μm ($\approx 2\delta_k$ at 600 Hz). The spacers run from the copper plates at ambient temperature along the edges of the stainless steel plates to the copper high temperature plates; the copper plates were therefore in the same plane as the stainless steel plates. The height of the stainless steel plates was 10 mm, that of the copper plates 1 mm. Their width varied linearly from 15 to 23 mm. Correspondingly, the width of the copper plates at the side of the resonator was 15 mm and at the high temperature end 23 mm. The total stack consists of 66 stainless steel spacers, 2×65 copper plates and 65 stainless steel plates; its total length was therefore 23 mm.

The linearly increasing width of the stack from 15 to 23 mm along the temperature gradient was chosen to compensate for the changing acoustic impedance conditions due to the temperature gradient. In a later stage of the research we found out that this was of minor importance for the function-

ing of the amplifier; this was confirmed by the computer model.

The cross section of the lower 20 mm of the high temperature end was square (23×23 mm), allowing proper connection to the stack. The upper 20 mm was circular (diameter 23 mm) and closed by a sliding piston, which allowed adjusting the total length L_{T_h} between 20 and 40 mm. This tuning was used to confirm model calculations experimentally and to optimize the amplification factor. The piston was sealed by a Viton O-ring to the column.

To obtain a good heat exchange between resonator, stack and piston carbon sheets were used and the three parts were firmly pressed together. The temperatures were controlled by temperature sensitive elements (PT-100). A temperature stabilized water flow was led around the ambient temperature part of the amplifier. Around the high temperature column an ''Inconel 600'' wire (length 1.25 m) was wound to obtain a uniform temperature over the column. This heating wire was shielded by a brass column. The high temperature part was stabilized to within 0.1 K with a Eurotherm 900 temperature controller.

IV. RESULTS

A. Loudspeaker experiments

For two different lengths of the high temperature column ($L_{T_h} = 20$ and 40 mm) its quality factor (Q) of the TAPA cell and the resonance frequency (ν) were determined for a range of temperatures ($T_h = 300-450$ K). The results of the calculations and the experiments, both for loudspeaker and laser experiments, are shown in Fig. 5. The inverse of the quality factor (Q^{-1}) shows a negative linear correlation to the applied temperature difference, i.e., Q increases with higher ΔT [Figs. 5(a) and 5(b)].[19] At the onset of self-oscillation the quality factor goes to infinity ($Q^{-1} \rightarrow 0$); the amplifier will maintain its oscillation since the work added to the gas is larger than the thermal and viscous losses. The resonance frequency shows a slight increase with ΔT which can be attributed to the increase of the speed of sound in the high temperature part of the column.

B. Trace gas experiments

The linearity of the TAPA cell was tested with a range of concentrations of ethylene in nitrogen between 2 and 34 ppm. These concentration were made in a dynamical gas mixing system with mass flow controllers (flow rate 5 L/h) and were calibrated against a certified mixture of 1.2 ppm of C_2H_4 in N_2. The PA signal was determined at the 10P14 and the 10P16 laser lines at three different temperatures of the TA amplifier ($L_{T_h} = 40$ mm). The results of these measurements are shown in Fig. 6. The corresponding Q values are included in Figs. 5(a) and 5(b).

A difference in Q value can be observed between the loudspeaker and laser experiments. This is due to dismounting of the TAPA cell in between these experiments.

Both theory and experiment show a linear relation between Q^{-1} and the applied temperature difference ΔT. Theory overestimates the Q value over the entire temperature range, and more significantly so toward higher temperatures. This is probably due to losses which are not included in the model. The model assumes a uniform temperature gradient along the stainless steel plates of the stack. Experimentally this uniform temperature distribution can only be ap-

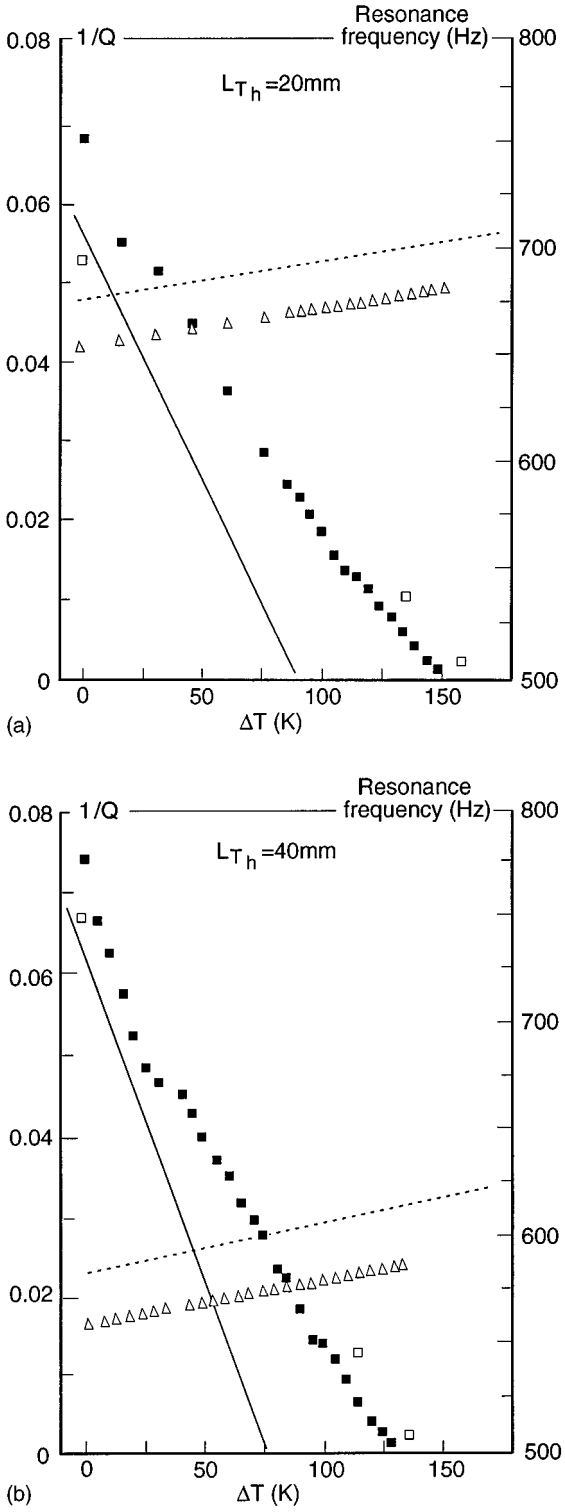

FIG. 5. Quality factor and resonance frequency are shown for two different column lengths $L_{T_h} = 20$ (a) and 40 mm (b). Loudspeaker experiments: Q value (■), resonance frequency (△); CO_2 laser experiments: Q value (□); theory: Q value (—), resonance frequency (---).

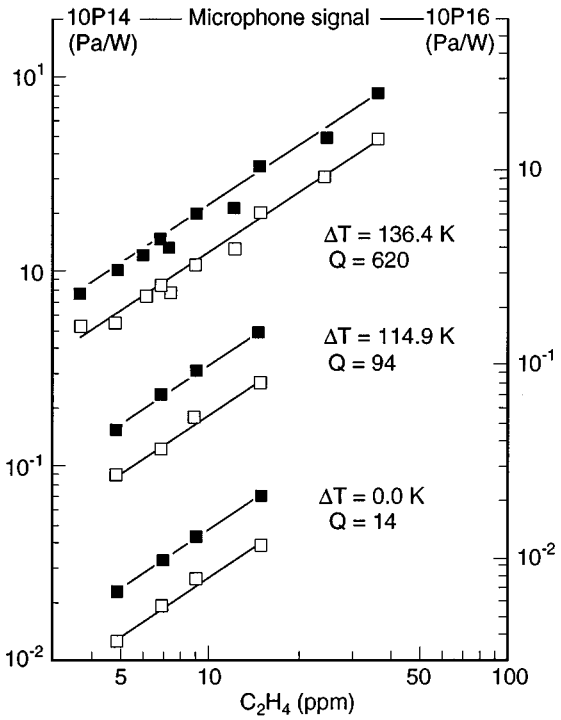

FIG. 6. Linearity of the PA signal as function of the ethylene concentration for three different temperature gradients along the stack ($L_{T_h}=40$ mm). 10P14 CO_2 laser line (■); 10P16 laser line (□).

proximated, causing a less effective acoustic amplification by the stack.

In Table II the cell constant F of the TAPA cell (in Pa cm/W; calculated from the PA signal[7] and a measure for overall detector sensitivity), its Q value and its resonance frequency are summarized for two different lengths ($L_{T_h}=20$ and 40 mm) and several temperature differences (ΔT). The values for an ordinary PA cell containing the same type of resonator but without amplifier section are added for comparison. Without temperature difference the resonance frequency of 565 Hz corresponds with a wavelength of 62 cm ($L_{T_h}=40$ mm). In the TAPA cell the distance from the closed end of the TA amplifier through the resonator to one of the open ends was 13.5 cm. This distance corresponds approximately to a quarter wavelength: the acoustic standing wave has its pressure nodes at the open ends of the resonator and its pressure antinode at the closed end.

TABLE II. Resonance frequency (ν), cell constant (F), and quality factor (Q) as function of high temperature column length (L_{T_h}) and temperature difference (ΔT) over the stack. The values for an ordinary photoacoustic cell containing the same type of resonator are added for comparison.

L_{T_h} (mm)	ΔT (K)	ν (Hz)	F (Pa cm/W)	Q
20	0	666.3	180	19.2±0.5
20	134.5	682.2	1050	101±2
20	159.4	687.4	5300	560±50
40	0	566.4	110	15.0±0.5
40	114.5	597.5	690	89±1
40	134.5	598.3	3960	430±30
Ordinary PA cell	NA	1093	2400	60±1

At $\Delta T=0$ a lower cell constant F and a lower Q value can be observed for $L_{T_h}=40$ mm as compared to $L_{T_h}=20$ mm. This is caused by: (i) increased surface area which induces larger thermal and heat conduction losses; (ii) a longer wavelength shift which moves the relative microphone position closer to the pressure node resulting in a lower microphone amplitude; and (iii) the volume increase of the TA amplifier. The intrinsic larger losses at $\Delta T=0$ are compensated by the larger gain, e.g., at $\Delta T=134.5$ K. Finally, self-oscillation for $L_{T_h}=40$ mm is obtained at a lower temperature difference than for the 20 mm column.

As shown in Table II a two times higher cell constant ($F=5300$ Pa cm/W) has been observed with TA amplification as compared to a normal PA cell ($F=2400$ Pa cm/W). At $\Delta T=0$ the cell constant was 13 times lower ($F=180$ Pa cm/W compared to 2400 Pa cm/W). This can be explained by the lower Q value (factor 4, due to a larger surface area), the larger volume (factor 2) and the nonoptimal position of the microphone along the standing acoustic wave (factor 1.4). The pressure antinode is at the end of the TA amplifier whereas for the normal PA resonator it is in front of the microphone.

The linearity of the detector for calibrated gas mixtures is demonstrated in Fig. 6 for several temperatures. The observed ratio of absorption strengths for C_2H_4 at the 10P14 and 10P16 CO_2 laser lines was constant with temperature and deviated less than 5% from the literature values.[20]

C. Discussion

As shown by the results the transmission line model describes the behavior of the TAPA cell fairly well. Therefore, we tried to extract optimum design criteria from the model.

The losses of the TA amplifier are observable at $\Delta T=0$. To start self-oscillation the gain introduced by the amplification must overcome the present acoustic losses; both gain and loss determine the final temperature of self-oscillation. To perform a constant TA amplification chopper frequency instability and temperature difference instability must be suppressed. A Q value of 1000 is considered a practical limit. A good cell design should lead to a low self-oscillation temperature and a high F over Q ratio.

Within the theoretical model we have put the TA amplifier at several places along the resonator tube; we could, however, not find a larger signal enhancement than at its place at the center. If the cross section of TA amplifier does not differ too much from twice the cross section of the resonator, the effective resonator length corresponds to the length of the acoustic resonator plus twice the length of the amplifier.

For optimal performance of the TA amplifier it is necessary to have an optimal heat exchange within the stack, i.e., an optimal ratio between the thermal boundary layer thickness and stack plate spacing. In Fig. 7 the calculated cell constant and quality factor are shown as a function of the temperature difference and the stack plate distance ($2y_0$). The thickness of the thermal boundary layer δ_k depends on the temperature (average value over the stack) and the resonance frequency. At $\Delta T=0$ the increase of the stack plate

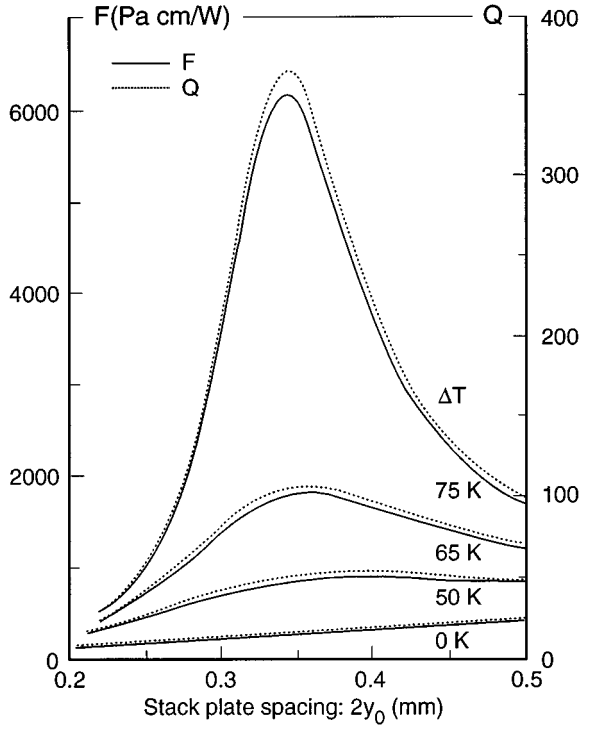

FIG. 7. Theoretical calculations for a TAPA cell with ($L_{T_h}=40$ mm). The resonator and ambient part of the stack are at 300 K. For four temperature differences over the stack the cell constant F and the quality factor Q are given as function of the distance (y_0) between the plates in the stack ($2y_0$). For N_2 at 300 K $\delta_\kappa=0.109$ mm (at 375 K $\delta_\kappa=0.132$ mm).

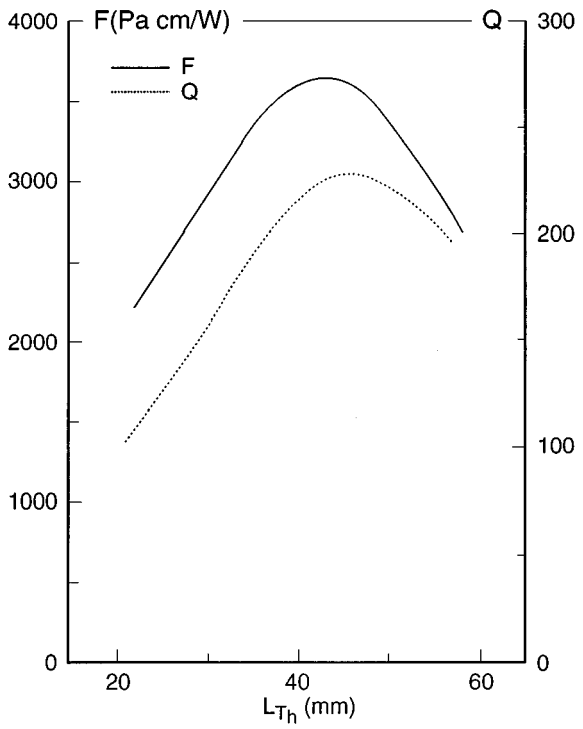

FIG. 8. Cell constant (F) and quality factor (Q) calculated as function of L_{T_h} ($\Delta T=75$ K). The dimensions of resonator and TA amplifier are same as used in the experiments given in Fig. 5.

spacing (Fig. 7) results in lower losses, i.e., higher Q and F values. At $\Delta T\neq 0$ optimum amplification is achieved at a stack plate spacing slightly larger than twice the thermal boundary layer; the latter is confirmed in the literature.[15,18]

The height and cross sectional area of the stack barely affect the amplification process; however, they do affect the losses. The losses are proportional to the stack height and inversely proportional to the cross section area; thus, a short height and a large cross section lead to optimal performance. However, this may be in conflict with the condition of maintaining a homogeneous temperature over the upper and lower surfaces of the stack; the heat conducting properties of the copper plates may be a shortcoming. With a given temperature difference a reduced stack height leads to a stronger gradient over the stack and thus to a larger heat transport. An increased cross section will limit the heat transport toward/from (high/low temperature end) the center and thus a cold/hot spot will appear. Other materials and other shapes of stack design can be considered, e.g., the recently introduced pin array stack design.[21]

From the model we found that amplification and loss are fairly independent of the shape of the cross section of the high temperature part. The volume of this high temperature part appears to be more critical. For a fixed temperature difference $\Delta T=75$ K the calculated results of changing L_{T_h} for the cell constant and the quality factor are shown in Fig. 8. As deduced from Fig. 5 the losses (Q value at $\Delta T=0$) for a small volume ($L_{T_h}=20$ mm) are less than for a larger volume ($L_{T_h}=40$ mm). However, the amplification (e.g., at $\Delta T=75$ K) for a small volume is also less and self-oscillation is reached at a somewhat higher temperature. From this we can conclude our initial choice for the length $L_{T_h}=40$ mm was appropriate.

The TAPA cell could serve in other fields of research as well. It allows to obtain very high Q values and then becomes extremely sensitive for resonance frequency shifts. High Q values are of importance when relaxation phenomena are observed; variation in relaxation rates cause a shift of the acoustical resonance frequency and changes the response function of an acoustical cavity.[22]

ACKNOWLEDGMENTS

The authors wish to express their thanks to M. Peters, H. Verscharen, and H. v. Brakel for technical support.

[1] L. B. Kreuzer, N. D. Kenyon, and C. K. N. Patel, Science **177**, 347 (1972).
[2] R. A. Rooth, A. J. L. Verhage, and L. W. Wouters, Appl. Opt. **29**, 3643 (1990).
[3] S. Bernegger and M. W. Sigrist, Infrared Phys. **30**, 375 (1990).
[4] P. L. Meyer and M. W. Sigrist, Rev. Sci. Instrum. **61**, 1779 (1990).
[5] F. J. M. Harren, J. Reuss, E. J. Woltering, and D. D. Bicanic, Appl. Spectrosc. **44**, 1360 (1990).
[6] F. G. C. Bijnen, J. H. P. Hackstein, P. Kestler, F. J. M. Harren, and J. Reuss, Laser Optoelectron. **2**, 68 (1995).
[7] F. G. C. Bijnen, F. J. M. Harren, and J. Reuss, Rev. Sci. Instrum. (in press).
[8] L. B. Kreuzer, J. Appl. Phys. **42**, 2934 (1971).
[9] R. Gerlach and N. M. Amer, Appl. Phys. **23**, 319 (1980).
[10] E. Nodov, Appl. Opt. **17**, 1110 (1978).
[11] E. Kritchman, S. Shtrikman, and M. Slatkine, J. Opt. Soc. Am. **68**, 1257 (1978).
[12] J. W. Strutt, *Lord Rayleigh, the Theory of Sound* (Dover, New York, 1877), Vol. II, p. 230.

[13] A. G. Bell, Am. J. Sci. **XX**, 305 (1880).
[14] W. P. Arnott, H. Moosmüller, R. E. Abbott, and M. D. Ossofsky, Rev. Sci. Instrum. **66**, 4827 (1995).
[15] K. W. Taconis, Physica **15**, 738 (1949).
[16] G. W. Swift, J. Acoust. Soc. Am. **84**, 1145 (1988).
[17] P. M. Morse and K. U. Ingard, in *Theoretical Acoustics* (McGraw–Hill, New York, 1968).
[18] S. Bernegger and M. W. Sigrist, Appl. Phys. B **44**, 234 (1987).
[19] A. A. Atchley, J. Acoust. Soc. Am. **92**, 2907 (1992).
[20] R. J. Brewer, C. W. Bruce, and J. L. Mater, Appl. Opt. **21**, 4093 (1982).
[21] G. W. Swift and R. M. Keolian, J. Acoust. Soc. Am. **94**, 941 (1993).
[22] A. Karbach and P. Hess, J. Chem. Phys. **84**, 2945 (1986).